water

MDPI

Article

The Cr(III) Exchange Mechanism of Macroporous Resins: The Effect of Functionality and Chemical Matrix, and the Statistical Verification of Ion Exchange Data

Khizar Hussain Shah [1], Noor S. Shah [2], Gul Afshan Khan [3], Sadaf Sarfraz [4], Jibran Iqbal [5], Aneeqa Batool [3], Ahmad Jwuiyad [6], Shabnam Shahida [7], Changseok Han [8,9] and Monika Wawrzkiewicz [10,*]

1 Department of Chemistry, COMSATS University Islamabad, Islamabad Campus, Park Road, Islamabad 45540, Pakistan; khizar_nce@yahoo.com
2 Department of Environmental Sciences, COMSATS University Islamabad, Vehari Campus, Vehari 61100, Pakistan; noorsamad@ciitvehari.edu.pk
3 Department of Chemistry, COMSATS University Islamabad, Abbottabad Campus, University Road, Abbottabad 22060, Pakistan; yahakhan.ga@gmail.com (G.A.K.); aneeqabatool1996@gmail.com (A.B.)
4 Department of Chemistry, Lahore Garrison University, Lahore 5400, Pakistan; dr.sadafsarfraz@lgu.edu.pk
5 College of Interdisciplinary Studies, Zayed University, Abu Dhabi 144534, United Arab Emirates; jibran.iqbal@zu.ac.ae
6 Department of Chemistry, College of Science, King Saud University, P.O. Box 2455, Riyadh 11451, Saudi Arabia; ahmedjuiead@gmail.com
7 Department of Chemistry, University of Poonch, Rawalakot 12350, Pakistan; shabnamshahida@upr.edu.pk
8 Department of Environmental Engineering, INHA University, Incheon 22212, Republic of Korea; hanck@inha.ac.kr
9 Program in Environmental & Polymer Engineering, Graduate School, INHA University, Incheon 22212, Republic of Korea
10 Department of Inorganic Chemistry, Institute of Chemical Sciences, Faculty of Chemistry, Maria Curie-Skłodowska University, M. Curie Skłodowska Sq. 2, 20-031 Lublin, Poland
* Correspondence: monika.wawrzkiewicz@mail.umcs.lublin.pl; Tel.: +48-81-537-57-38

Abstract: This study focuses on investigating and comparing the influence of the surface functional groups and chemical matrices of macroporous resin on the Cr(III) exchange mechanism. The results discussed herein indicate that sulfonic resin removed Cr(III) ions with faster kinetics than carboxylic resin. Equilibrium was established within 15 and 7 min for the carboxylic and sulfonic resins, respectively, with a 99.5% removal efficiency at 333 K. The Langmuir exchange capacity was observed to be higher for the sulfonic resin (1.5 mmol·g^{-1}) than the carboxylic resin (0.80 mmol·g^{-1}) at 333 K. The adsorption isotherms obtained for the carboxylic and sulfonic resins were H and S types, respectively, representing a higher affinity of the carboxylic resin for Cr(III) removal at a low metal ion concentration. Additionally, it was noted that the carboxylic resin preferentially co-sorbed H^+ and $Cr(OH)^{2+}$ ions below Cr(III) concentrations of 6–8 mmol.L^{-1}. The H+ ions co-sorption was almost negligible, whereas the Cr(III) exchange was 87 and 34.5% for the carboxylic acid resin and sulfonic acid resins, respectively. The data of the concentration studies were evaluated using non-linear forms of Freundlich, Langmuir, and Dubinin–Radushkevich adsorption isotherm models, and the kinetic data were analyzed using pseudo-Ist- and pseudo-IIst-order kinetic models. The activation energy E_a for Amberlite IRC-50 (Na^+) was greater (22.4 kJ·mol^{-1}) than that of Amberlyst-15 (Na^+) 17 kJ·mol^{-1}, indicating a higher energy barrier for the ion exchange reaction on carboxylic resin. As per the findings of a statistical error analysis (RMSE and SSE) and absolute average relative distribution (AARD) statistical model, a close agreement between the experimental and theoretical values suggested that the Langmuir isotherm was well-fitted to the current adsorptive investigations. The interaction of the COO^- and SO^{3-} functional sites of the resins for the exchange of Cr(III) ions was validated through an FT-IR analysis. The macroporous resins used in the current study for Cr(III) exchange showed promising performances compared to other resins. The current investigations revealed valuable insights for choosing macroporous resins as adsorbents in water filtration systems.

check for updates

Citation: Shah, K.H.; Shah, N.S.; Khan, G.A.; Sarfraz, S.; Iqbal, J.; Batool, A.; Jwuiyad, A.; Shahida, S.; Han, C.; Wawrzkiewicz, M. The Cr(III) Exchange Mechanism of Macroporous Resins: The Effect of Functionality and Chemical Matrix, and the Statistical Verification of Ion Exchange Data. *Water* **2023**, *15*, 3655. https://doi.org/10.3390/w15203655

Academic Editor: Laura Bulgariu

Received: 6 September 2023
Revised: 7 October 2023
Accepted: 12 October 2023
Published: 18 October 2023

Keywords: adsorption; chromium ion; resins; ion exchange; water treatment

1. Introduction

Chromium is a heavy metal that exists in two stable oxidation states, i.e., Cr (III) and Cr(VI), with Cr(III) being the most common form occurring in the environment [1,2]. Cr(III) can be considered as beneficial and an important food supplement at a low level, playing a fundamental role in biochemical reactions, but its existence in the ecosystem exceeding the recommended 0.05 $mg \cdot L^{-1}$ level can also cause significant health hazards [3,4]. In addition, the presence of different oxidizing agents such as Fe_2O_3, MnO_2, and $NaNO_3$ in the environment can result in the rapid oxidation of Cr(III) into more hazardous Cr(VI) under alkaline conditions [5]. Therefore, both the removal and recovery of Cr(III) and Cr(VI) from industrial wastes are compulsory preceding their direct discharge into the aquatic system. By performing this, environmental pollution risks will be significantly reduced, and recovering Cr(III) compounds for reuse will be economically advantageous.

Based on scrutinizing the literature, several technologies have been employed for the removal of different contaminants and pollutants from aqueous bodies, such as chemical precipitation, advance oxidation, membrane filtration, photocatalystic degradation, adsorption, and ion exchange [6]. Among all these removal techniques, ion exchange is a highly promising, competitive, well-developed, and widely used technique because of its high removal efficiency, quick kinetics, simple design, cheap operating costs, and regeneration of both adsorbent and adsorbate [7]. Although, the adsorption of metal ions by ion exchangers is mostly a result of ion exchange processes, it is also, however, controlled by significant factors including porosity, matrix structure, the nature and type of functional groups, the mobility of exchangeable ions, and the moisture contents of the resin [8,9]. Therefore, information on such factors is mandatory for providing guidelines on the assessment of suitable ion exchange resins as adsorbents during drinking and waste waters treatment [10–16].

To our knowledge, no comprehensive research has been published so far to clarify the potential impact of variations in resin's structural properties on its metal exchange sorption properties. Recently, Edebali and Pehlivan evaluated the potential of different cationic exchange resins of XUS43578, CR1, and HCR-W2 C-160 for the extraction of Cu(II) ions and the results showed that the extraction efficiency was significantly affected by the structure, type of charged functional groups, and other physiochemical characteristics of the resin [17]. Similar to this, Xiao et al. assessed the efficacy of various polyacrylic resins (D730, D314, 312, and 213) for Cr(III) removal and reported a significant influence of functional groups on the resin's capacity for exchange and adsorption behavior [12].

In recent years, macroporous ion exchange resins with a greater porosity and large surface areas have received great attention due to their excellent mechanical and thermal stability, which makes them a good choice of adsorbent in the field of ion exchange technology [12]. The distinguishing feature of macroporous resin lies in its network of large pores extending throughout the whole body of the resin matrix. Given that the diffusion coefficient of the adsorbed ion depends on the relative dimensions of the ion and the pores in the resin, this unique structure of macroporous structures enables the exchange reaction to proceed rapidly [13,14].

The present study aims to examine the ability of two distinct macroporous cation exchange resins, Amberlite IRC-50 (a weak acid resin) and Amberlyst-15 (a strong acid), to bind Cr(III), based on the functionality of the resin and the structure of the matrix. It is essential to mention that we are reporting, for the first time, deep insights and important chemistry regarding the Cr(III) exchange mechanism on strong-polystyreme-based and weak-polyacrylic-based macacroporous resins. The valuable knowledge presented in this work will be fruitful for the implementation of macroporous resins for Cr(III), as well as other metal ions encountered in aquatic media.

The most important objectives of the current research work were to: (1) investigate the effect of time, temperature, concentration, and pH of metal ion solutions, (2) investigate the influence of H^+ ions co-sorption, (3) explain the removal efficiency and underlying mechanisms on the basis of the functionality and matrix structure of the resins, (4) evaluate the ion exchange data using different non-linear isotherm and kinetic models, (5) undertake a statistical error analysis (RMSE and SSE) to verify several adsorption isotherm and kinetic models, and (6) use an absolute average relative distribution (AARD) statistical model to verify several adsorption isotherm models. The current investigation will serve as a guide for choosing and optimizing the best macroporous resin for future projects involving the treatment of water and wastewater solutions.

2. Materials and Methods

Chemicals with analytical grade purity were utilized to prepare the solutions and reagents, and distilled water was thoroughly used in all the preparations. All the chemicals, including $CrCl_3 \cdot 6H_2O$ and the cation exchange resins such as Amberlite IRC-50(H^+) and Amberlyst-15(H^+), were bought from BDH Chemicals Ltd. (Poole, UK) and used as received.

2.1. Cr (III)-Containing Solutions

The primary stock solution comprising 19.32 mmol·L^{-1} of Cr(III) was prepared by mixing an appropriate amount of chromium chloride ($CrCl_3 \cdot 6H_2O$) with 1000 mL of deionized water. The subsequent secondary solutions, with concentration values ranging from 0.96 to 19.23 mmol·L^{-1}, were prepared by diluting the primary stock solution.

2.2. Conversion of H^+ Form of Resins into Na^+ Form

Ten grams of each virgin form of macroporous resin was taken into separate columns and treated with the excess 0.1 M NaCl solution to convert them into Na^+ forms. To completely saturate the resins with the sodium ions, the H^+ form of the resin was held in contact with the sodium chloride solution until the effluent concentration became equal to 0.1 M. After that, repeated washings of the Na^+ forms of the resins with triply distilled water were carried out before drying at 393 K for a time duration of 24 h. Finally, the dried resin samples were kept in glass-stoppered bottles for further utilization in adsorption experiments.

2.3. Analysis of Cr (III)

The amount of chromium ions, i.e., Cr(III), left in the solution phase after the adsorption studies was analyzed using an Atomic Absorption Spectrophotometer (model no. Perkin Elmer AAS 800, PerkinElmer Instruments, Shelton, CT, USA) with a flame mode. The amount of Cr(III) ions exchanged per unit mass of the adsorbent resin was calculated using the well-known mass balance Equation (1):

$$X = \frac{V(C_i - C_e)}{1000\ m} \quad (1)$$

where X (mmol·g^{-1})—the amount of chromium ions, i.e., Cr(III) sorbed onto the resin, C_i (mmol·L^{-1})—the initial concentration of chromium ions, C_e (mmol·L^{-1})—the equilibrium concentration of chromium ions, V (L)—the volume of the solution, and m (g)—the mass of the adsorbent resin.

2.4. Ion Exchange Studies

Studies on equilibrium were conducted using the batch adsorption technique. In 100 mL conical flasks, 30 mL of adsorbate solutions containing Cr(III) ions at known concentrations (0.96, 1.92, 3.85, 5.77, 7.69, 9.62, 11.54, 13.46, 15.38, and 19.23 mmol·L^{-1}) were taken; in total, 0.2 g of adsorbent resin was added to each flask. These suspensions were agitated in a thermostat shaker bath operating at a stirring speed of 120 rpm at 293–333 K. At equilibrium time, i.e., after a duration of 2 h, the suspension's equilibrium

pH was recorded, the suspension was then filtered, and the amount of Cr(III) metal ions in the residue was analyzed according to the method outlined above. For the kinetics analysis, the infinite bath method was employed, i.e., by mixing 3 g of resin with 100 mL of a 19.23 mmol·L^{-1} Cr(III) solution in a double-walled glass beaker, connected with a water-circulating bath, at a controlled temperature (293–333 K) and a stirring speed of 120 rpm. At regular time intervals, 1 mL from the reaction assembly was extracted and analyzed for Cr(III) ion uptake.

Adsorption isotherms were used to determine the relationships between adsorbate ions and adsorbents. The obtaining of different parameters from isotherms enables us to understand the adsorption mechanism in detail, the chemistry of the surface, and the capability of the adsorbent to uptake the adsorbate. The equilibrium process of Cr(III) exchange on both the carboxylic acid resin and sulfonic acid resin was described by employing various adsorption isotherms, i.e., Langmuir, Freundlich, and Dubinin–Radushkevich models [15–21]. A nonlinear regression analysis is a procedure for fitting adsorption data into an equation [22,23].

Langmuir isotherms deal with the monolayer adsorption of adsorbate molecules due to the presence of homogeneous surfaces with finite and equivalent surface sites on the adsorbate surface. The Langmuir adsorption model can be expressed in the following nonlinear form [24]:

$$q_e = \frac{q_m K_L C_e}{1 + K_b C_e} \quad (2)$$

where C_e (mmol·L^{-1})—the equilibrium concentration of Cr(III) ions, q_e and q_m (mmol·g^{-1})—the sorption capacities at the equilibrium and maximum sorption capacity, respectively, and K_L (L·g^{-1})—the Langmuir adsorption constant.

The Freundlich isotherm deals with heterogeneous surfaces, but it is limited to the description of adsorption data in a limited range only, such as at high and intermediate concentrations [25]. It also gives us an indication about the favorability of adsorption [26] and describes the nature of the adsorption, such as when the n is equal to 1, which describes that there is linear adsorption, whereas a value greater than 1 describes physical adsorption and less than 1 describes the chemical process of adsorption occurring [22]. This model suggests that the adsorption energy decreases exponentially after the occupation of the adsorption active centers of an adsorbent [27]:

$$q = K_F C_e^{1/n} \quad (3)$$

where C_e (mmol·L^{-1})—the equilibrium concentration of Cr(III) ions, K_F ($mg^{1-1/n}$ $L^{1/n}$·g^{-1})—the constant associated with the adsorption capacity of the adsorbent, exhibiting the affinity between the adsorbate molecules, and n—the constant associated with the sorption intensity, implicating the effect of the metal ion concentration (when with values of n > 1, it exhibits favorable adsorption conditions).

The Dubinin–Radushkevich (D-R) isotherm model is an alternative practiced model which primarily expresses an adsorption procedure succeeding a pore-filling contrivance. Heterogeneous and homogenous surface adsorption phenomena are generally explained by this model. The Dubinin–Radushkevich isotherm non-linear model can be expressed as Equations (4) and (5) [28]:

$$q_e = q_s exp\left(-K_{DR}\varepsilon^2\right) \quad (4)$$

$$\varepsilon = RTln\left(1 + \frac{1}{C_e}\right) \quad (5)$$

where q_e and q_m (mmol·g^{-1}) —in the D–R isotherm model signify the equilibrium and maximum adsorption capacity, K_{DR} (mol^2/kJ^2)—the constant describing the adsorption mean free energy, ε (kJ·mol^{-2})—the adsorption potential, R (J·mol^{-1}·K^{-1})—the characteristic constant related to the general gas constant, and T (K)—the absolute temperature.

Since the nature of the adsorption is determined by the strength of the interaction between the adsorbate and adsorbent, the free energy of the adsorption was thus determined to find the amount of energy used to transfer the adsorbate from an infinity of the solution to the surface of the adsorbent using Equation (6):

$$E = \frac{1}{\sqrt{2K_{DR}}} \tag{6}$$

where E ($kJ \cdot mol^{-1}$)—the energy of the adsorption.

When the value of E is less than 8 $kJ \cdot mol^{-1}$, then physical adsorption occurs, whereas energy values in the range between 8 $kJ \cdot mol^{-1}$ and 16 $kJ \cdot mol^{-1}$ indicate either chemical adsorption or ion exchange, and E being bigger than 16 $kJ \cdot mol^{-1}$ suggests that particle diffusion governs the reaction [27].

There are numerous models which can be utilized to explain the kinetics of adsorption, but currently, pseudo-Ist-order and pseudo-IInd-order models (Equations (7) and (8)) were used to analyze the order of the ion exchange reaction [29]. The literature findings reveal that the pseudo-Ist-order kinetic model is mainly used to portray sorption kinetics and the below-mentioned equation is used to find desired results [30–33]. The pseudo-Ist-order reaction is non-linearly expressed as:

$$q_t = q_e\left(1 - e^{-k_1 t}\right) \tag{7}$$

where k_1 (min^{-1})—the pseudo-Ist-order rate constant and q_e and q_t—the amounts of adsorbate species retained by the resin at equilibrium and at any time t, respectively.

In addition to the Ist-order kinetic data, the pseudo-IInd-order kinetic model was used to evaluate the adsorption kinetic data, as given below. It is assumed that the pseudo-IInd-order model possessed a rate-limiting step, which is expected to be chemisorption in nature:

$$q_t = \frac{k_2 q_e^2 t}{1 + k_2 q_e t} \tag{8}$$

where k_2 ($mmolg^{-1} \cdot min^{-1}$)—the rate constant for the pseudo-IInd-order equation [34].

The activation energy (E_a) values were calculated by using the well-known Arrhenius equation:

$$n\frac{k_2}{k_1} = -\frac{E_a}{RT}\left[\frac{1}{T_2} - \frac{1}{T_1}\right] \tag{9}$$

where k_1 and k_2 are the rate constant values at a lower (T_1) and higher temperature (T_2), respectively, and R is a general gas constant.

2.5. Statistical Verification of Adsorption Data and Isotherm Models

The coherence between the experimental and calculated data was determined by assessing, with R^2 adjusted, the error of the root mean square (RMSE) and the sum of square error (SSE) as follows [35]:

$$RMSE = \sqrt{\frac{\sum_{n=1}^{i}\left(q_{i,exp} - q_{i,cal}\right)^2}{n}} \tag{10}$$

where $q_{i,exp}$—the value determined experimentally, $q_{i,cal}$—the value of q predicted by the fitted model, and n—the number of experiments performed.

To further assess the accuracy of the adsorption isotherm models and the absolute average relative deviation percentage (AARD), a statistical model was used, and this model can be described as follows:

$$AARD = \frac{1}{N}\sum_{i=1}^{N}\frac{\lceil q_e - q_t \rceil}{q_e} \tag{11}$$

where N—the number of data points, q_e—the experimentally calculated adsorption capacity, and q_t—the theoretical adsorption capacity.

2.6. FT-IR Analysis

To prepare the samples for the FTIR analysis, each macroporous resin sample, before and after the adsorption of Cr(III), was completely mixed and ground with potassium bromide (1:100 ratio). The powdered mixture was then made into transparent discs by placing them into a hydraulic press. The samples before and after the adsorption were subjected to an FT-IR analysis using a Shimadzu infrared spectrometer (Model 8202PC).

3. Results

3.1. Exchange Kinetics

To avoid curve overlapping, the kinetic curves for the Cr(III) ion sorption of the macroporous resins are shown in Figure 1 at the lowest and highest temperatures (293 and 333 K).

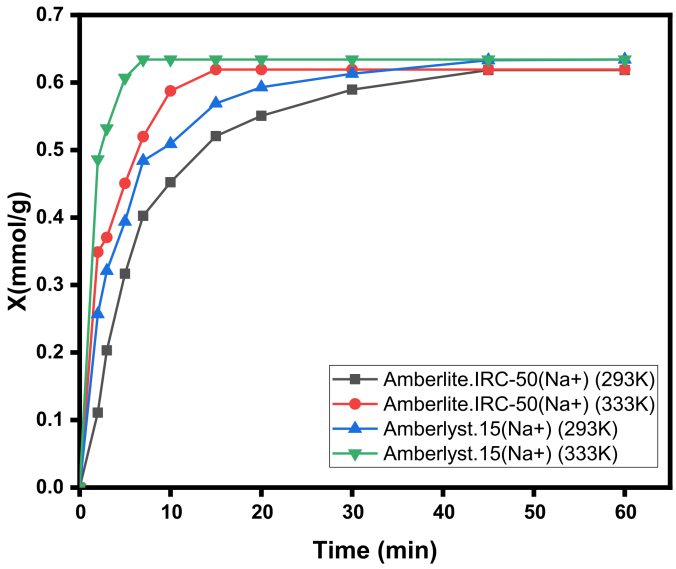

Figure 1. Kinetic curves for Cr(III) exchange at 293 and 333 K.

This demonstrates that the kinetics of the Cr(III) exchange onto these resins was increased with an increasing solution time and solution temperature. Equilibrium was established at 45, 30, and 15 min for the carboxylic resin and 45, 20, and 7 min for the sulfonic resin at 293, 313, and 333 K, respectively. This figure also reveals that the rate of exchange initially remained higher because of numerous available active sites for Cr(III) ion sorption. However, after a certain time, due to the lack of free active sites, the rate of sorption for Cr(III) ions slowed down. The general kinetics trend observed by these resins was ranked Amberlyst-15 (Na^+) > Amberlite IRC-50(Na^+). This indicated that the rate of chromium exchange was faster for the sulfonic resin as compared to the carboxylic resin, which had a low dissociation constant. Similar conclusions were made by Riveros et al. for Fe(III) sorption on methacrylic carboxylic resin [19].

3.2. Changes in pH Values during Exchange Studies

A comparative plot of the changes in the solution pHs during the Cr(III) sorption for both resins at two different temperatures (293 and 333 K) is also shown in Figure 2.

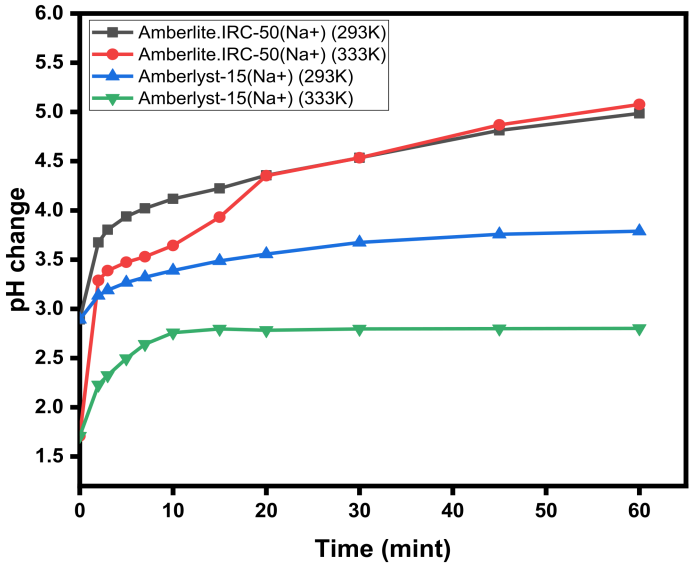

Figure 2. Kinetic curves for pH changes during Cr(III) exchange at 293 and 333 K.

It was observed that the initial solution pH for the Cr(III) solution of 19.23 mmol·L^{-1} decreased from 2.9 to 1.7 and from 3.3 to 2.8 with the increasing temperature, since, at elevated temperatures, the hydrolysis of Cr(III) was increased according to Equation (12). The pH value was observed to increase over time during the Cr (III) exchange on both the carboxylic and sulfonic resins. This increasing solution pH after the adsorption studies was evident of the fact that these resins removed both $Cr(OH)^{+2}$ and H^+ ions, as evident from the following reactions (12–17):

$$Cr^{3+} + H_2O \leftrightarrow Cr(OH)^{2+} + H^+ \quad (12)$$

$$RCOONa^+ + H^+ \leftrightarrow RCOOH + Na^+ \quad (13)$$

$$2RCOONa + Cr(OH)^{2+} \leftrightarrow R(COO)_2Cr(OH) + 2Na^+ \quad (14)$$

$$RSO_3Na + H^+ \leftrightarrow RSO_3H + Na^+ \quad (15)$$

$$2RSO_3Na + Cr(OH)^{2+} \leftrightarrow (RSO_3)_2Cr(OH) + 2Na^+ \quad (16)$$

$$3RNa + Cr^{3+} \leftrightarrow R_3Cr + 3Na^+ \quad (17)$$

Furthermore, the co-sorption of H^+ at the start appeared to be very rapid in comparison to the Cr (III) adsorption. While comparing Figures 1 and 2, this process seems to be more evident for the carboxylic acid resin. This indicated that, at the beginning of the ion exchange reaction, the exchange of H^+ with Na^+ ions occurred according to Equation (13), and thus exceeded when the hydrogen form of the resins interacted with $Cr(OH)^{+2}$, following Equation (14). However, the responsible reaction mechanism for the sulfonic acid resin seems to be according to Reaction (17). The same ion exchange mechanism has also been suggested by other researchers for the removal of Cr(III) [26,32]. It is also notable from the figure that the co-sorption of H^+ ions was greater for the carboxylic acid resin in comparison to the sulfonic acid resin. This can be explained by the weakly acidic nature of the carboxylic resin having a high affinity for hydrogen ions.

3.3. Influence of Concentration and Temperature

The comparative Cr(III) adsorption isotherms for the exchange on the carboxylic verses sulfonic resins at varying temperatures, i.e., 293–333 K, are shown in Figure 3, which demonstrates that the chromium adsorption onto these exchangers was increased during an increase in the solution temperature and initial concentration of metal ions.

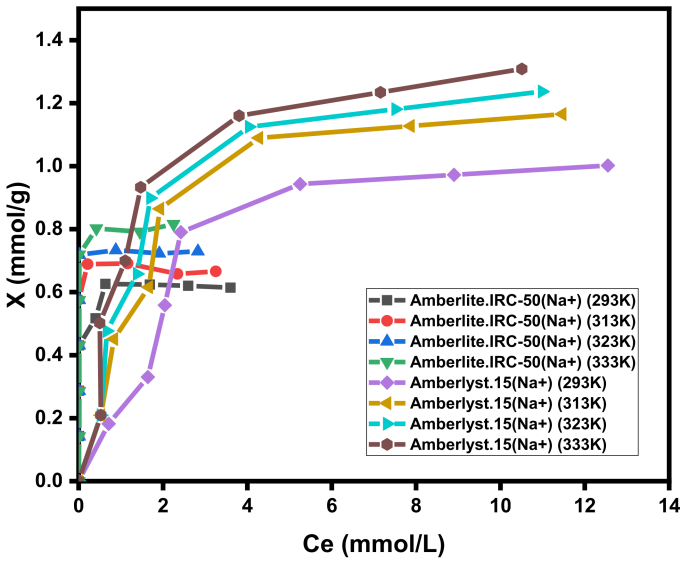

Figure 3. Cr(III) adsorption isotherms at different temperatures.

In the current investigation, the shapes of the adsorption isotherms can be classified into two categories according to the Giles classification scheme: H and S types [29]. For Amberlite IRC-50(Na^+), H-types of sorption isotherms were observed, which indicates the high affinity for Cr(III) ions at low concentrations of metal ions and a maximum surface coverage of the resin. The adsorption isotherms obtained for the sulfonic acid resin were only S types, which indicates the low affinity of Cr(III) at low concentrations in comparison to the carboxylic resin. This may have been because of the higher tendency of the sulfonic acid resin for exchangeable sodium ions. However, the increasing concentration of metal ions would provide a driving force to replace Na^+ ions for Cr(III) exchange.

The maximum exchange capacities for these resins were enhanced with an increasing temperature of the Cr(III) solution. Respective increases in Cr(III) were observed from 0.62 to 0.76 mmol·g^{-1} for the carboxylic acid resin and from 1.13 to 1.40 mmol·g^{-1} for the sulfonic acid resin when the temperature increased from 293 to 333 K. The greater exchange capacity of the sulfonic resin compared to the carboxylic resin was highly linked to the charged functional group and matrix structure of the resins.

3.4. Influence of H^+ Ions Co-Sorption

The results for the influence of the H^+ co-sorption on the Cr(III) exchange for both the resins are given in Figure 4, depicting a relationship between ΔpH $\left(pH_{eq} - pH_i\right)$ versus the amount of Cr(III) exchanged at 293 K.

It can be predicted from the figure that, for both exchangers, ΔpH > 0 indicates the co-sorption of H^+ and Cr $(OH)^{2+}$ ions according to Equations (12)–(15). A higher value of ΔpH was observed only for the carboxylic acid resin, which indicated that this resin had a remarkable affinity for H^+ ions as compared to the sulfonic acid resin. It is very interesting to observe from Figure 4 significant and valuable information related to the intersection point when the ΔpH value for the sulfonic resin nearly reaches zero, representing that H^+ ion co-sorption was almost nonexistent. It can be also be noted that H^+ co-sorption became almost insignificant by extrapolating the ΔpH values to zero, whereas Cr(III) sorption was 87 and 34.5% for the carboxylic acid resin and sulfonic acid resin, respectively. However, at a

higher temperature (333 K), this threshold point was never achieved; hence, the co-sorption of H^+ ions was observed to increase for both resins under investigation.

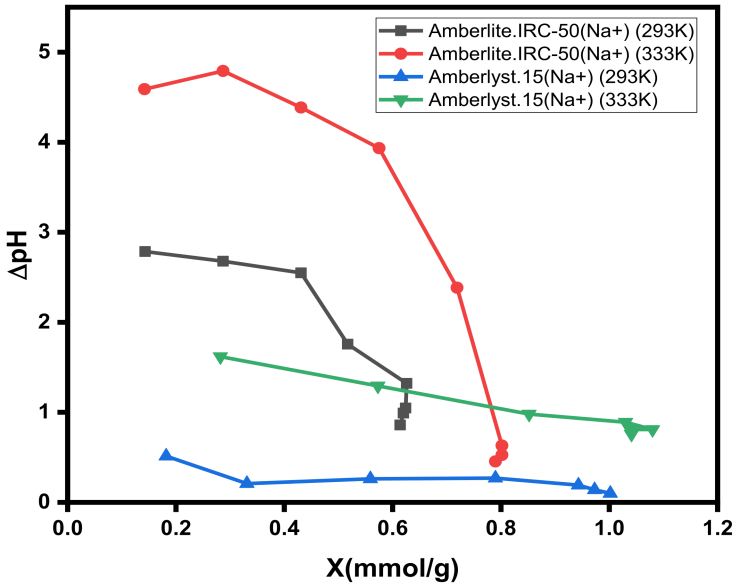

Figure 4. ΔpH versus Cr(III) exchange X(mmol/g) for different resins.

To find out the effect of the Cr(III) initial metal ion concentration on the co-sorption of H^+ ions, the ΔpH values were also plotted against the initial concentrations of Cr(III), as shown in Figure 5. It can be observed from Figure 5 that the H^+ co-sorption was decreased with increasing Cr(III) initial concentrations. A very sharp decline in the pH curves for the carboxylic acid resin suggests that the Cr(III) concentrations had a significant impact on the H^+ co-sorption. This also demonstrated that the carboxylic acid resin had a substantially higher co-sorption below chromium concentrations of 6–8 mmol·L^{-1} in comparison to the sulfonic acid resin. The major reason for this behavior might have been a higher tendency of carboxylic active sites for H^+ ions in the case of the former, as discussed in the preceding section. Similar results were also obtained at 333 K.

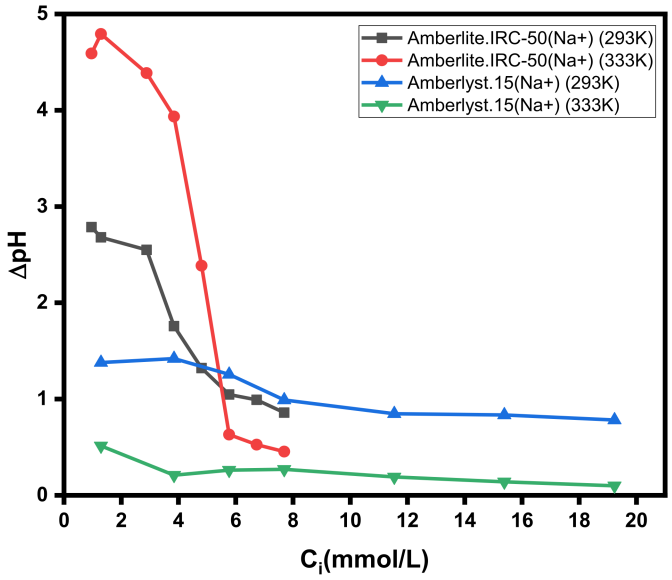

Figure 5. ΔpH versus C_i (mmol/L) for different resins.

3.5. Ion Exchange Data Modeling

The Langmuir, Freundlich, and D–R adsorption parameters, along with an error analysis, are given in Table 1. It can be observed from the table that the maximum adsorption capacities determined from all the isotherm models were enhanced with an increase in the temperature, facilitating the exchange of Cr(III) onto the surface of the resins [32,33]. It is evident that the Langmuir isotherm showed the best fit for Cr(III) exchange onto both the resins, with a high R^2_{adj}, low RMSE, and SSE among other two parameter isotherms. The calculated value of q_e was 0.60 mmol·g^{-1}, which is closer to the experimental q_e value of 0.62 mmol·g^{-1}, for the carboxylic acid resin at 293 K, and the sulfonic acid resin had q_e = 1.29 mmol·g^{-1} with an R^2 of 0.76, which is greater than the Freundlich model. The results for the AARD model are illustrated in Figure 6. According to the findings, the correlated ability was computed in the order of the Langmuir, D–R model, and Freundlich isotherms, respectively. The AARD values for the Langmuir adsorption isotherm, Freundlich isotherm, and DR models were found to be 2.199, 6.144, and 9.8, respectively. It is evident from Figure 6 that, for the Langmuir adsorption isotherm, AARD had the lowest value, demonstrating that this model was the best-fitted as compared to the other adsorption isotherm models. Based on the R^2, RMSE, SEE, and AARD values, it can be suggested that the possibility of monolayer formation was a result of Cr(III) exchange onto the homogeneous surface sites of macroporous resins. Similar conclusions have been made by other researchers [26,32].

Table 1. Langmuir, Freundlich, and D–R isotherm parameters for Cr(III) exchange on Amberlite IRC-50 (Na^+) and Amberlyst-15 (Na^+).

Models		**Amberlite IRC-50 (Na^+)**				**Amberlyst-15 (Na^+)**			
		Temperature				**Temperature**			
		293 K	313 K	323 K	333 K	293 K	313 K	323 K	333 K
Langmuir	$q_{e,exp}$	0.62	0.65	0.72	0.80	0.97	1.12	1.18	1.23
	$q_{e,cal}$	0.60	0.67	0.74	0.80	1.29	1.40	1.45	1.49
	K_L	80.077	377.14	104.02	0.71	0.373	0.57	0.67	0.79
	R^2	0.874	0.811	0.710	0.685	0.76	0.82	0.86	0.88
	RMSE	0.073	0.107	0.149	0.152	0.093	0.076	0.081	0.099
	SSE	0.05	0.104	0.178	0.210	0.076	0.046	0.054	0.079
Freundlich									
	$q_{e,cal}$	0.64	0.69	0.73	0.79	0.96	1.10	1.18	1.24
	K_F	0.56	0.65	0.69	0.75	0.40	0.54	0.59	0.64
	N	2.49	10.95	9.40	8.29	2.49	2.79	2.87	2.99
	R^2	0.85	0.77	0.65	0.64	0.70	0.76	0.79	0.81
	RMSE	0.078	0.118	0.155	0.16	0.131	0.129	0.136	1.146
	SSE	0.056	0.12	1.20	0.23	0.138	0.135	1.148	1.171
D-R									
	$Q_{e,cal}$	0.61	0.69	0.74	0.81	1.03	1.15	1.20	1.26
	E	8.88	12.51	8.08	8.87	0.90	1.39	1.58	1.81
	R^2	0.87	0.81	0.70	0.70	0.95	0.97	0.97	0.95
	RMSE	0.28	0.33	0.29	0.39	0.56	0.61	0.65	0.68
	SSE	0.74	1.00	0.69	1.56	2.58	3.03	3.38	3.72

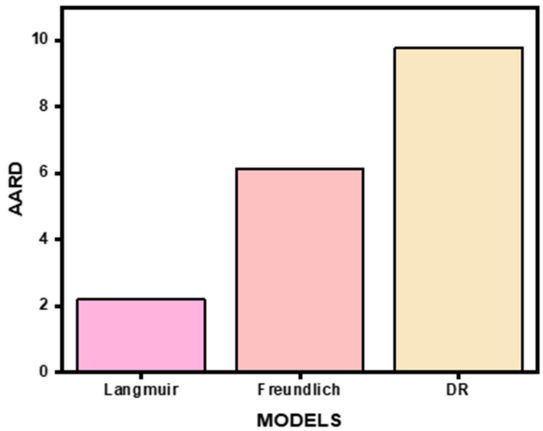

Figure 6. AARD for different isotherm models.

3.6. Adsorption Isotherm Parameters

The adsorption parameters of the Langmuir, Freundlich, and D–R isotherms can be predicted in Table 1. The q_e values obtained for various resins were observed to follow the given order, i.e., $q_{eAmberlyst\text{-}15(Na^+)} > q_{eAmberlite\ IRC\text{-}50(Na^+)}$ which is the same as discussed in the preceding sections for the sorption isotherms and can be correlated to the effect of the charged functional group and the matrix of the adsorbent. The lower q_e values for the Amberlite IRC-50 resin can be attributed to the weak acidic nature of the carboxylic groups. However, for the K_L values, a reverse trend was observed, i.e., $K_{LAmberlite\ IRC\text{-}50(Na^+)} > K_{LAmberlyst\text{-}15(Na^+)}$ which demonstrates that the K_l values for the carboxylic acid resin were higher than those for the sulfonic acid resin, whereas the lower K_L values for Amberlyst-15 indicated a poor interaction between Cr(III) and the sulfonic acid group (SO_3^-) and the higher K_L values for Amberlite IRC-50 suggested a stronger binding of Cr(III) ions with the carboxylic acid group (COO^-). These findings are consistent with several investigations that have been published earlier [36–38]. The value of E for Amberlite IRC-50 (Na^+) was greater than 8 kJ·mol^{-1}, i.e. in the range varying from 8.5 to 12 kJ·mol^{-1}, indicating an ion exchange mechanism, whereas for Amberlyst-15 (Na^+), the value of E was less than 8 kJ·mol^{-1} and indicated that weak forces of interaction were involved in the adsorption process [37,38].

3.7. Kinetic Data Modeling

The plots of the pseudo-Ist-order and -IIst-order kinetic models on both resins are shown in Figure 7. According to the value of R^2, the pseudo-second-order is more applicable, but as an error analysis method such as RMSE and SSE is applied. The RMSE and SSE value was smaller for the pseudo-Ist-order as compared to the pseudo-IIst-order [14]. Therefore, the pseudo-Ist-order was considered to be more applicable for Cr(III) exchange on both resins, as shown by the proximity of the estimated and observed values for q_e. The increase in the k_1 values with temperature assures that the reaction was endothermic [29].

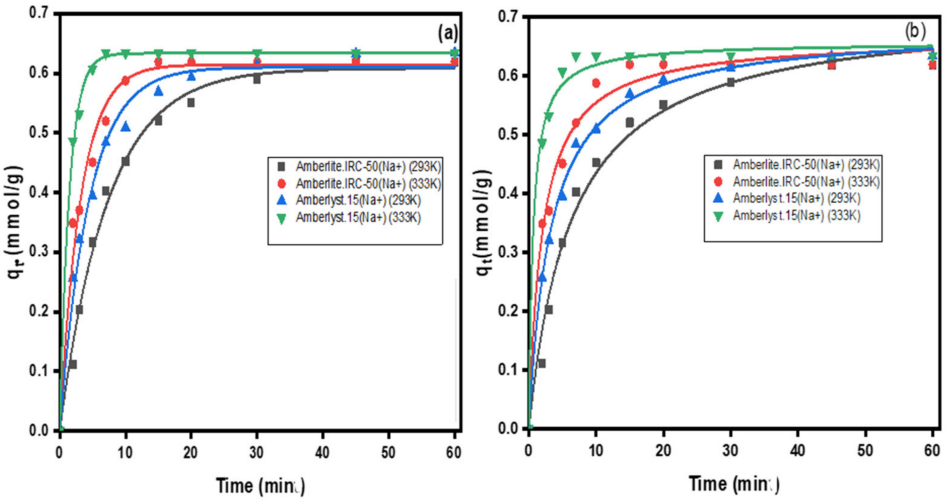

Figure 7. Fitting of the pseudo-Ist order (**a**) and pseudo-IInd order (**b**) equations to kinetic sorption data.

3.8. Rate Constant and Activation Energy Parameters

Table 2 lists the calculated values of the rate constants (k) determined at two different temperatures (293 and 333 K). The pseudo-first-order rate constant values were obtained in the following order, $k_{Amberlyst\text{-}15(Na+)} > k_{Amberlite\ IRC\text{-}50(Na+)}$, which is parallel to the previously discussed order for the kinetic curves.

Table 2. Kinetic parameters of the pseudo-Ist- and pseudo-IInd-order equation for Cr(III) exchange on different macroporous resins.

Kinetic Model	T (K)	k_1 (min)$^{-1}$	R^2	SSE	RMSE
Pseudo-Ist-order					
Amberlite IRC-50 (Na^+)	293	0.13	0.99		
	333	0.31	0.98	0.01	0.11
Amberlyst-15 (Na^+)	293	0.22	0.98		
	333	0.67	0.99	0.02	0.15
Pseudo-IInd-order	T (K)	k_2(mmolg^{-1}·min^{-1})	R^2	SSE	RMSE
Amberlite IRC-50 (Na^+)	293	0.21	0.98		
	333	0.75	0.98	0.05	0.23
Amberlyst-15 (Na^+)	293	0.44	0.99		
	333	2.47	0.99	0.04	0.20

The resins' activation energies were obtained in the following order: $E_{a\ Amberlyst\text{-}15(Na^+)} > E_{a\ Amberlit\ .IRC\text{-}50(Na^+)}$. This suggested that a temperature rise was accompanied by an increase in the co-sorption of H^+ ions, resulting in an increase in the pH of the solution. As a result, the activation energy values were decreased. The noticeable pK_a value for the carboxylic acid resin was found to be 5.47 [36]. The increase in the pH of the solution not only promoted an increase in the degree of ionization of the carboxylic acid groups, but also lowered the energy of the activation required by the resin to bind Cr(III) ions.

3.9. FT-IR Analysis of Cr(III) Exchange Mechanism

Figure 8a depicts the results of the FT-IR spectroscopic analysis of the carboxylic and sulfonic acid resins before and after the Cr(III) ion exchange. The IR-spectra for the Amberlite IRC-50 (Na^+) resin before the Cr(III) exchange show a characteristic peak occurring at 1392 cm^{-1}, attributed to the C-O symmetric stretching vibration in the carboxylic functional group of the virgin resin [36–38]. After the loading of Cr(III), the C-O peak at 1392 cm^{-1} was shifted to 1384 cm^{-1}, suggesting the involvement of the COO^- group in the Cr(III) adsorption. Similar results for binding mechanisms have also been suggested elsewhere [14]. The FTIR spectra of the sulfonic acid resin Amberlyst-15 (Na^+) before and after the exchange of Cr(III) are presented in Figure 8b. The spectrum of the virgin resin before the exchange of Cr(III) shows characteristic peaks at 1005, 1030, 1095, and 1123 cm^{-1}, assigned to the S=O stretching vibrations of the sulfonic functional group, as well as the in-plane bending vibrations of an aromatic ring attached to the sulfonic acid group. Peaks at 1128 and 1091 cm^{-1} were found to exhibit a lower intensity after Cr(III) adsorption, whereas peaks at 1010 and 1039 cm^{-1} were found to undergo a smaller shift, only by a few less cm^{-1}, reflecting the exchange of Cr(III) ions with SO_3^-. A similar mechanism for metal ion sorption by sulphonic acid resins was also found elsewhere [35–38].

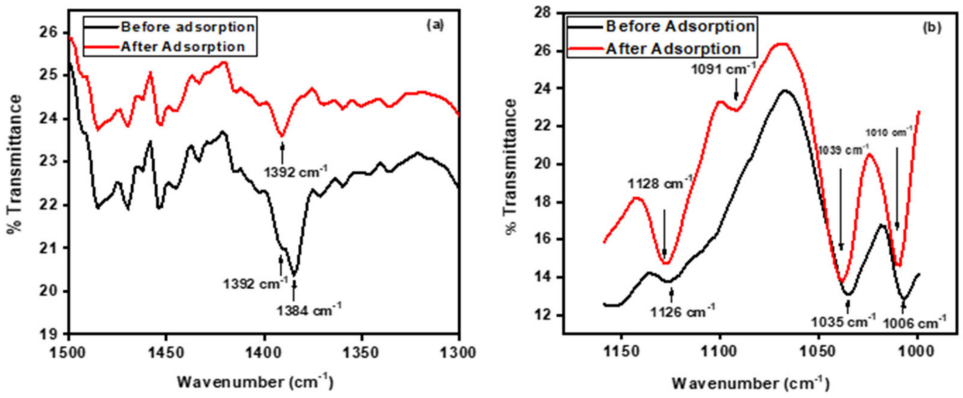

Figure 8. (**a**) FT-IR spectra of Amberlite IRC-50 (Na^+) before and after Cr(III) exchange, and (**b**) FT-IR spectra of Amberlyst-15 (Na^+) before and after Cr(III) exchange.

4. Conclusions

From the explanation above, it can be inferred that the functionality and matrix structure of resins have a significant impact on their ability to remove Cr(III) ions from aqueous solutions. The overall exchange capacity of the sulfonic acid resin was found to be greater than that of the carboxylic resin due to its strong acidic character. However, at very low metal ion concentrations, the carboxylic acid resin performed well as compared to Amberlyst-15, which showed a better performance at higher metal ion concentrations. The carboxylic resin was found to be more selective towards H^+ ions co-sorption in comparison to the sulfonic resin, and this co-sorption was found to be greater at low metal ion concentrations and solution temperatures. A close agreement between the $q_{e,cal,}$ and $q_{e,exp}$ values, the statistical analysis (RMSE and SSE), and the absolute average relative distribution (AARD) statistical model proved that Langmuir models showed the best fitting for the adsorption data. The greater K_L values for the carboxylic resin indicated a comparatively strong electrostatic interaction of Cr(III) with the COO^- functional groups rather than $SO_3{}^-$. Studies using FT-IR measurements proved that weak electrostatic interactions of the metal ion with the carboxylic and sulfonic acid groups were present in the resins.

Author Contributions: Conceptualization, K.H.S.; methodology, K.H.S., G.A.K. and A.B.; formal analysis, N.S.S., A.B. and S.S. (Sadaf Sarfraz).; investigation, G.A.K. and S.S. (Sadaf Sarfraz).; resources, N.S.S., J.I. and A.J.; data curation, K.H.S. and S.S (Shabnam Shahida); writing—original draft preparation, K.H.S., G.A.K. and A.B.; writing—review and editing, N.S.S., J.I., A.J., C.H. and M.W.; visualization, N.S.S., C.H. and M.W., supervision, K.H.S. and S.S.; funding acquisition, K.H.S., A.J. and C.H. All authors have read and agreed to the published version of the manuscript.

Funding: This research was funded by; (1) Higher Education Commission (HEC) of Pakistan under NRPU Grant No: 8817; (2) Researchers Supporting Project Number (RSPD2023R584), King Saud University, Riyadh, Saudi Arabia; and (3) The National Research Foundation of Korea (NRF) grant funded by the Korean government (MSIT) (No. 2021R1A2C1093183). The authors gratefully acknowledge financial support from these grants.

Institutional Review Board Statement: Not applicable.

Informed Consent Statement: Not applicable.

Data Availability Statement: Data will be available on request.

Acknowledgments: The authors acknowledge the following institutes for supporting this study: (1) Higher Education Commission (HEC) of Pakistan under NRPU Grant No: 8817; (2) Researchers Supporting Project Number (RSPD2023R584), King Saud University, Riyadh, Saudi Arabia; and (3) The National Research Foundation of Korea (NRF) grant funded by the Korean government (MSIT) (No. 2021R1A2C1093183). The authors gratefully acknowledge financial support from these grants.

Conflicts of Interest: The authors declare no conflict of interest.

References

1. Jiang, Z.; Chen, K.; Zhang, Y.; Wang, Y.; Wang, F.; Zhang, G.; Dionysiou, D.D. Magnetically recoverable $MgFe_2O_4$/conjugated polyvinyl chloride derivative nanocomposite with higher visible-light photocatalytic activity for treating Cr (VI)-polluted water. *Sep. Purif. Technol.* **2020**, *236*, 116272. [CrossRef]
2. Ge, T.; Shen, L.; Li, J.; Zhang, Y.; Zhang, Y. Morphology-controlled hydrothermal synthesis and photocatalytic Cr (VI) reduction properties of α-Fe_2O_3. *Colloids Surf. A Physicochem. Eng. Asp.* **2022**, *635*, 128069. [CrossRef]
3. Hsueh, Y.-H.; Lin, K.-S.; Wang, Y.-T.; Chiang, C.-L. Copper, nickel, and zinc cations biosorption properties of Gram-positive and Gram-negative MerP mercury-resistance proteins. *J. Taiwan Inst. Chem. Eng.* **2017**, *80*, 168–175. [CrossRef]
4. Yadav, S.K.; Sinha, S.; Singh, D.K. Chromium (VI) removal from aqueous solution and industrial wastewater by modified date palm trunk. *Environ. Prog. Sustain. Energy* **2015**, *34*, 452–460. [CrossRef]
5. Naushad, M.; Al-Othman, Z.A.; Islam, M. Adsorption of cadmium ion using a new composite cation-exchanger polyaniline Sn (IV) silicate: Kinetics, thermodynamic and isotherm studies. *Int. J Environ. Sci. Technol.* **2013**, *10*, 567–578. [CrossRef]
6. Frei, R.; Polat, A. Chromium isotope fractionation during oxidative weathering—Implications from the study of a Paleoproterozoic (ca. 1.9 Ga) paleosol, Schreiber Beach, Ontario, Canada. *Precambrian Res.* **2013**, *224*, 434–453.

7. Khan, S.A.; Abbasi, N.; Hussain, D.; Khan, T.A. Sustainable mitigation of paracetamol with a novel dual-functionalized pullulan/kaolin hydrogel nanocomposite from simulated wastewater. *Langmuir* **2022**, *38*, 8280–8295. [CrossRef]
8. Khan, S.A.; Siddiqui, M.F.; Khan, T.A. Ultrasonic-assisted synthesis of polyacrylamide/bentonite hydrogel nanocomposite for the sequestration of lead and cadmium from aqueous phase: Equilibrium, kinetics and thermodynamic studies. *Ultrason. Sonochemistry* **2020**, *60*, 104761. [CrossRef]
9. Bleotu, I.; Dragoi, E.N.; Mureşeanu, M.; Dorneanu, S.A. Removal of Cu (II) ions from aqueous solutions by an ion-exchange process: Modeling and optimization. *Environ. Prog. Sustain. Energy* **2018**, *37*, 605–612. [CrossRef]
10. Jadbabaei, N.; Zhang, H. Sorption mechanism and predictive models for removal of cationic organic contaminants by cation exchange resins. *Environ. Sci. Technol. Lett.* **2014**, *48*, 14572–14581. [CrossRef]
11. Alvarado, L.; Torres, I.R.; Chen, A. Integration of ion exchange and electrodeionization as a new approach for the continuous treatment of hexavalent chromium wastewater. *Sep. Purif. Technol.* **2013**, *105*, 55–62. [CrossRef]
12. Xiao, K.; Han, G.; Li, J.; Dan, Z.; Xu, F.; Jiang, L.; Duan, N. Evaluation of polyacrylic anion exchange resins on the removal of Cr (VI) from aqueous solutions. *RSC Adv.* **2016**, *6*, 5233–5239. [CrossRef]
13. Wang, W.; Li, X.; Yuan, S.; Sun, J.; Zheng, S. Effect of resin charged functional group, porosity, and chemical matrix on the long-term pharmaceutical removal mechanism by conventional ion exchange resins. *Chemosphere* **2016**, *160*, 71–79. [CrossRef] [PubMed]
14. Zhu, Z.; Zhang, M.; Liu, F.; Shuang, C.; Zhu, C.; Zhang, Y.; Li, A. Effect of polymeric matrix on the adsorption of reactive dye by anion-exchange resins. *J. Taiwan Inst. Chem. Eng.* **2016**, *62*, 98–103. [CrossRef]
15. Murtaza, B.; Naseer, A.; Imran, M.; Shah, N.S.; Al-Kahtani, A.A.; ALOthman, Z.A.; Shahid, M.; Iqbal, J.; Abbas, G.; Natasha, N. Chromium removal from aqueous solution using bimetallic Bi^0/Cu^0-based nanocomposite biochar. *Environ. Geochem. Health* **2023**, 1–14. [CrossRef]
16. Murtaza, B.; Bilal, S.; Imran, M.; Shah, N.S.; Shahid, M.; Iqbal, J.; Khan, Z.U.H.; Ahmad, N.; Al-Kahtani, A.A.; ALOthman, Z.A. The Study of Removal Chromium (VI) ions from Aqueous Solution by Bimetallic ZnO/FeO Nanocomposite with Siltstone: Isotherm, Kinetics and Reusability. *Inorg. Chem. Commun.* **2023**, *154*, 110891. [CrossRef]
17. Edebali, S.; Pehlivan, E. Evaluation of chelate and cation exchange resins to remove copper ions. *Powder Technol.* **2016**, *301*, 520–525. [CrossRef]
18. Ren, J.; Zheng, Y.; Lin, Z.; Han, X.; Liao, W. Macroporous resin purification and characterization of flavonoids from *Platycladus orientalis* (L.) Franco and their effects on macrophage inflammatory response. *Food Funct.* **2017**, *8*, 86–95. [CrossRef]
19. Riveros, P. The extraction of Fe (III) using cation-exchange carboxylic resins. *Hydrometallurgy* **2004**, *72*, 279–290. [CrossRef]
20. Cavaco, S.A.; Fernandes, S.; Augusto, C.M.; Quina, M.J.; Gando-Ferreira, L.M. Evaluation of chelating ion-exchange resins for separating Cr (III) from industrial effluents. *J. Hazard. Mater.* **2009**, *169*, 516–523. [CrossRef]
21. Özmetin, C.; Aydın, Ö.; Kocakerim, M.M.; Korkmaz, M.; Özmetin, E. An empirical kinetic model for calcium removal from calcium impurity-containing saturated boric acid solution by ion exchange technology using Amberlite IR–120 resin. *Chem. Eng. J.* **2009**, *148*, 420–424. [CrossRef]
22. Vargas, A.M.; Cazetta, A.L.; Kunita, M.H.; Silva, T.L.; Almeida, V.C. Adsorption of methylene blue on activated carbon produced from flamboyant pods (*Delonix regia*): Study of adsorption isotherms and kinetic models. *Chem. Eng. J.* **2011**, *168*, 722–730. [CrossRef]
23. Babaei, A.A.; Baboli, Z.; Jaafarzadeh, N.; Goudarzi, G.; Bahrami, M.; Ahmadi, M. Synthesis, performance, and nonlinear modeling of modified nano-sized magnetite for removal of Cr (VI) from aqueous solutions. *Desalin. Water Treat.* **2015**, *53*, 768–777. [CrossRef]
24. Thitame, P.V.; Shukla, S.R. Removal of lead (II) from synthetic solution and industry wastewater using almond shell activated carbon. *Enviorn. Prog. Sustain. Energy* **2017**, *36*, 1628–1633. [CrossRef]
25. Ng, C.; Losso, J.N.; Marshall, W.E.; Rao, R.M. Freundlich adsorption isotherms of agricultural by-product-based powdered activated carbons in a geosmin–water system. *Bioresour. Technol.* **2002**, *85*, 131–135. [CrossRef]
26. Brdar, M.; Šćiban, M.; Takači, A.; Došenović, T. Comparison of two and three parameters adsorption isotherm for Cr (VI) onto Kraft lignin. *Chem. Eng. J.* **2012**, *183*, 108–111. [CrossRef]
27. Vijayakumar, G.; Tamilarasan, R.; Dharmendirakumar, M. Adsorption, Kinetic, Equilibrium and Thermodynamic studies on the removal of basic dye Rhodamine-B from aqueous solution by the use of natural adsorbent perlite. *J. Mater. Environ. Sci.* **2012**, *3*, 157–170.
28. Dubinin, M. The equation of the characteristic curve of activated charcoal. *Proc. USSR Acad. Sci.* **1947**, *55*, 327–329.
29. Sadeghalvad, B.; Khosravi, S.; Azadmehr, A.R. Nonlinear isotherm and kinetics of adsorption of copper from aqueous solutions on bentonite. *Russ. J. Phys. Chem. A* **2016**, *90*, 2285–2291. [CrossRef]
30. Ahmadi, S.; Igwegbe, C.A.; Rahdar, S.; Asadi, Z. The survey of application of the linear and nonlinear kinetic models for the adsorption of nickel (II) by modified multi-walled carbon nanotubes. *Appl. Water Sci.* **2019**, *9*, 98. [CrossRef]
31. Rivas, B.L.; Pooley, S.A.; Maturana, H.A.; Villegas, S. Metal ion uptake properties of acrylamide derivative resins. *Macromol. Chem. Phys.* **2001**, *202*, 443–447. [CrossRef]
32. Gode, F.; Pehlivan, E. A comparative study of two chelating ion-exchange resins for the removal of chromium (III) from aqueous solution. *J. Hazard. Mater.* **2003**, *100*, 231–243. [CrossRef] [PubMed]

33. Dubey, S.; Gusain, D.; Sharma, Y.C. Kinetic and isotherm parameter determination for the removal of chromium from aqueous solutions by nanoalumina, a nanoadsorbent. *J. Mol. Liq.* **2016**, *219*, 1–8. [CrossRef]
34. Ho, Y.-S.; McKay, G. Sorption of dye from aqueous solution by peat. *Chem. Eng.* **1998**, *70*, 115–124. [CrossRef]
35. Markandeya, S.; Kisku, G. Linear and non-linear kinetic modeling for adsorption of disperse dye in batch process. *Res. J. Environ. Toxicol.* **2015**, *9*, 320–331.
36. Fei, W.; Wang, L.-J.; Li, J.-S.; Sun, X.-Y.; Han, W.-Q. Adsorption behavior and mechanism of cadmium on strong-acid cation exchange resin. *Trans. Nonferrous Met. Soc. China* **2009**, *19*, 740–744.
37. Jha, M.K.; Van Nguyen, N.; Lee, J.-c.; Jeong, J.; Yoo, J.-M. Adsorption of copper from the sulphate solution of low copper contents using the cationic resin Amberlite IR 120. *J. Hazard. Mater.* **2009**, *164*, 948–953. [CrossRef]
38. Salem, I.A. Activation of H_2O_2 by Amberlyst-15 resin supported with copper (II)-complexes towards oxidation of crystal violet. *Chemosphere* **2001**, *44*, 1109–1119. [CrossRef]